



THE UNIVERSITY *of* EDINBURGH

Edinburgh Research Explorer

The Study of Different Unidirectional IPOS Connected DC-DC Converters for Wind Farm Based Multi-Connected DC System

Citation for published version:

Rong, X, Shek, JKH & Macpherson, E 2021, 'The Study of Different Unidirectional IPOS Connected DC-DC Converters for Wind Farm Based Multi-Connected DC System', *International Transactions on Electrical Energy Systems*, vol. 31, no. 5, e12855. <https://doi.org/10.1002/2050-7038.12855>

Digital Object Identifier (DOI):

[10.1002/2050-7038.12855](https://doi.org/10.1002/2050-7038.12855)

Link:

[Link to publication record in Edinburgh Research Explorer](#)

Document Version:

Publisher's PDF, also known as Version of record

Published In:

International Transactions on Electrical Energy Systems

General rights

Copyright for the publications made accessible via the Edinburgh Research Explorer is retained by the author(s) and / or other copyright owners and it is a condition of accessing these publications that users recognise and abide by the legal requirements associated with these rights.

Take down policy


The University of Edinburgh has made every reasonable effort to ensure that Edinburgh Research Explorer content complies with UK legislation. If you believe that the public display of this file breaches copyright please contact openaccess@ed.ac.uk providing details, and we will remove access to the work immediately and investigate your claim.



RESEARCH ARTICLE

WILEY

The study of different unidirectional input parallel output series connected DC-DC converters for wind farm based multi-connected DC system

Xiaoyun Rong | Jonathan K. H. Shek  | D. Ewen Macpherson

Institute for Energy Systems, School of Engineering, University of Edinburgh, Edinburgh, UK

Correspondence

Jonathan K. H. Shek, Institute for Energy Systems, School of Engineering, University of Edinburgh, Edinburgh EH9 3DW, UK.
Email: j.shek@ed.ac.uk

Summary

There is increasing interest in interconnecting individual wind turbines in offshore wind farms using DC networks rather than AC networks. However, the output voltage from each turbine/generator is normally low (less than 6 kV), so DC-DC converters are required to step-up the voltage to an intermediate level to interconnect the turbine outputs. Another DC-DC converter is required to step-up this intermediate voltage to a high level for transmission to the shore. The DC-DC converter applied to step-up the voltage from an intermediate voltage to a high level not only needs to operate with high voltage at both input and output, but also be capable of transferring hundreds of megawatts power. In these circumstances, Input Series Input Parallel Output Series (ISIPOS) DC-DC converter structure is a good option for the application. In this paper, three different kinds of Input Parallel Output Series (IPOS) DC-DC converters are presented and compared, and it is the first time this comparison has been made. Both the simulation and downscaled hardware test results are provided and analysed, while the best option in different situations is suggested.

KEYWORDS

control, DC-DC converter, HVDC, IPOS, ISIPOS, offshore wind farms, single active bridge, three phase

List of Symbols and Abbreviations: n_{SAB_ub} , turns ratio of the SAB converter in the SAB + Three-Phase Bridge IPOS converter structure; n_{TP_ub} , turns ratio of the Three-Phase Bridge converter in the SAB + Three-Phase Bridge IPOS converter structure; n_{TP_b} , turns ratio of the Three-Phase converter; V_{in_bT} , Input Voltage of Identical Three-Phase Bridge IPOS Converter; V_{in_ub} , Input Voltage of SAB + Three-Phase Bridge IPOS Converter; V_{in_bS} , Input Voltage of Identical SAB IPOS Converter; $V_{o_ub_SAB}$, Output Voltage of the SAB Converter in SAB + Three-Phase Bridge IPOS Converter Structure; $V_{o_ub_TP1,2}$, Output Voltages of the Three-Phase Bridge Converters in SAB + Three-Phase Bridge IPOS Converter Structure; $V_{o_bT_TP1,2,3}$, Output Voltages of the Three-Phase Bridge Converters in Identical Three-Phase Bridge IPOS Converter Structure; $V_{o_bS_SAB1,2,3}$, Output Voltages of the SAB Converters in Identical SAB IPOS Converter Structure; $I_{o_ub_SAB}$, Output current of the SAB converter in SAB + Three-Phase Bridge IPOS converter structure; $I_{o_ub_TP1,2}$, Output currents of the Three-Phase Bridge converters in SAB + Three-Phase Bridge IPOS converter structure; I_{o_ub} , Output current of the SAB + Three-Phase Bridge IPOS converter; $I_{o_bT_TP1,2,3}$, Output currents of the Three-Phase Bridge converters in Identical Three-Phase Bridge IPOS converter structure; I_{o_bT} , Output current of the Identical Three-Phase Bridge IPOS converter; $I_{o_bS_SAB1,2,3}$, Output currents of the SAB converters in Identical SAB IPOS converter structure; I_{o_bS} , Output current of the Identical SAB IPOS converter; ISIPOS, input series input parallel output series; IPOS, input parallel output series; PMSG, permanent magnet synchronous generator; PWM, pulse width modulation; SAB, single active bridge; ZCS, zero current switching; FFT, fast Fourier transform algorithm; EMF, Electromotive Force.

This is an open access article under the terms of the Creative Commons Attribution License, which permits use, distribution and reproduction in any medium, provided the original work is properly cited.

© 2021 The Authors. *International Transactions on Electrical Energy Systems* published by John Wiley & Sons Ltd.

1 | INTRODUCTION

In recent decades, offshore wind power has developed rapidly ever since the first offshore wind farm was commissioned in Denmark in 1991.¹ Offshore wind farms can generate large amounts of energy, but far away from the onshore consumption centres. There are two main ways to transfer large amounts of electrical energy over long distances: HVAC and HVDC. Compared with HVAC, for long-distance (greater than 50 km) power transmission and asynchronous system connection, HVDC submarine cables have overwhelming advantages.²⁻⁴ At present, the connection between each wind turbine and the main offshore hub is still normally AC, with AC to DC conversion at the hub and a single point to point HVDC submarine cable connected between the offshore hub and onshore power system, for example, the voltage source converter based DC system.^{5,6} This type of system has to take the AC synchronization into consideration, while the transmission voltage level is also limited.

The application of high-power DC-DC converter in the offshore wind system can be a way to solve the synchronization issues. Although DC-DC converters have been used in low and medium voltages, it is still a challenge to operate them with high voltage.^{4,7} Based on the situation, special reviews or study of high-power high-voltage DC-DC converter in offshore wind environment are needed, and already attract attention in different aspects like structure studies under high-voltage offshore wind environment, special control methods of converter itself, or simplified wind farm system with DC transmission.^{4,7-10}

In this paper, an innovative multi-terminal HVDC system with several levels of DC voltage, which is an alternative way to transfer the large amount of wind energy from offshore to the onshore system is proposed. The structure of this type of system can be seen in Figure 1. In the figure, each wind turbine has a permanent magnet synchronous generator (PMSG), where the AC output is rectified by a pulse width modulation (PWM) rectifier, before the connection with the DC-DC converter. The output voltage from the PWM rectifier is stepped up before the multi-terminal connection, while another high-power high-voltage DC-DC boost converter is applied to accumulate all the generated power from the wind farm before the long-distance transmission to shore. In Figure 1, the transmission distance is set to be 100 km, which is a typical distance for offshore wind farms in northeast Scotland.¹¹

The high-power, high-voltage 200 to 1000 MW DC-DC converter in Figure 1 cannot be a single DC-DC converter structure due to both the voltage and power limitations of the semiconductor devices, such as IGBTs¹² and transformer cores.¹³ As things stand, the input series input parallel output series (ISIPOS) structure, which is constructed with a number of individual converters, is necessary for the 50 kV to 400 kV step-up DC-DC converter.

When building a system in a far offshore environment, at a time of no wind, approximately 1% of the rated turbine power is required to be fed back from the onshore power system for the control and any other auxiliary circuits.¹⁴ However, the use of a converter with an ISIPOS bidirectional structure not only doubles the number of switches, increasing the complexity of the system and its control circuit, but also needs a much larger inductor connected at the primary side of the converter.¹⁴ In these circumstances, a unidirectional power transfer ISIPOS converter structure with separate anti-parallel connected low-power converter is a better solution for the system under the black start, as well as other feedback functions. The separate low-power converter is not discussed in detail in this paper.

In this paper, based on the converters study in Reference 14, three different unidirectional converter structures for the 50 to 400 kV DC-DC converter are studied. The identical Three-Phase Bridge and identical single active bridge (SAB) are minor deformations of the converters in other studies,^{8,10,15} while the SAB + Three-Phase Bridge is a new

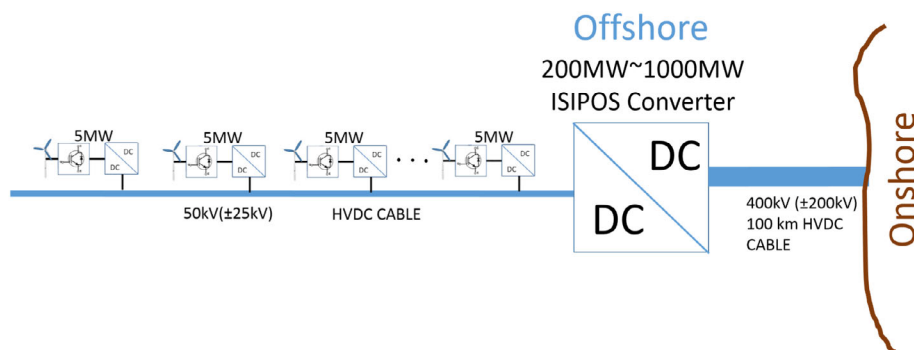


FIGURE 1 Simplified diagram of the multi-connected system

topology proposed by the authors. Both the simulation and downscaled hardware testing results of all the converters are presented and analysed in this paper, and the applications of all of them are suggested. This research also helps authors to do future works about the detailed system study of the whole offshore wind farm based multi-terminal DC system, which does not have many similarity study yet.

2 | THREE DIFFERENT PROSPECTIVE STRUCTURES OF THE ISIPOS CONNECTED CONVERTER FOR LARGE OFFSHORE WIND POWER TRANSMISSION

In this paper, for the ISIPOS converter, several combined structures using the SAB converter with primary side inductor and Three-Phase DC-DC converter are studied.

The high-power, high-voltage SAB hard-switching converter with primary side inductor (Figure 2) has only slightly higher losses than that of the Series Load Resonant converter, while the application of the SAB converter reduces the difficulty on the transformer design.¹⁶ Another valuable property of the SAB converter, if working in the discontinuous mode, is zero current switching (ZCS) can be achieved easily during switch on.¹⁷ Compared with the SAB converter with an inductor on the secondary side, it also decreases the manufacture difficulty of a high-voltage inductor.

The high-power, high-voltage, three-phase DC-DC converter applied for the ISIPOS structure, as shown in Figure 3,¹⁸ has two important advantages, especially under high-power conditions:

1. High-power transfer ability;
2. Low ripple content.

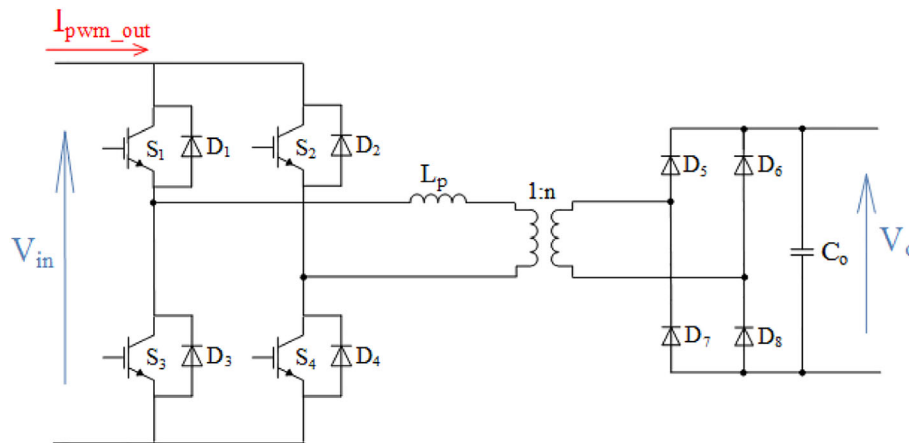


FIGURE 2 Single active bridge (SAB) converter

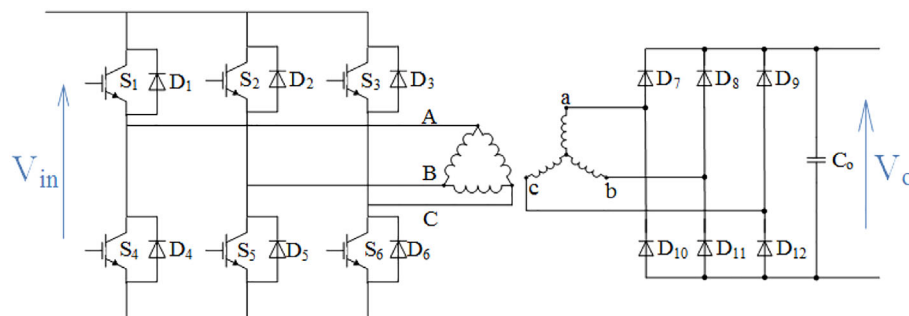


FIGURE 3 Three-phase bridge converter

Under the same power and voltage conditions, the transformer and passive filters are smaller, compared with other galvanic isolated DC-DC converters.¹⁸

Regarding the connection method of the three-phase transformer, the delta-star structure can be the best option, because:

1. Operational issues caused by the leakage inductance and copper losses are reduced. In this study, Three-Phase Bridge DC-DC converters are used to step-up the voltage, and the delta-star transformer requires a lower turns ratio than other constructions.
2. Delta-star configuration has both the lowest transformer power rating and switch current rating¹⁸;
3. Circulating current caused by multiples of third harmonics on the closed delta winding can help to reduce the distortion of the induced EMF.¹⁹

The design method¹⁷ and simulation study of both the SAB converter with primary side inductor and the Three-Phase Bridge DC-DC converter under high-power high-voltage conditions have been presented in detail in Reference 14, as well as their downscaled hardware testing. In this paper, the values of all the parameters and components used for both converters are listed directly, when looking into the operation of the different ISIPOS converter structures.

As mentioned in Section 1, the unidirectional ISIPOS structure is a better solution for the 50 to 400 kV DC-DC converter in Figure 1, compared to the bidirectional converter. Varying the connection method between the SAB converter with primary side inductor and the Three-Phase Bridge DC-DC converter, three different unidirectional ISIPOS converter structures can be obtained, as shown in Figure 4, where n and j are integer numbers.

If categorizing the three different ISIPOS structures by controllability, Figure 4A-C can be described as a partially input voltage controllable converter, open-loop controlled converter and fully input voltage controllable converter, respectively. It should be noticed that the structures in Figure 4A,B are modelled based on the ideas in other research studies,^{8,10,15} while the structure in Figure 4C is a new topology proposed by the authors. Important information about the converters in Figure 4 can be concluded as follows:

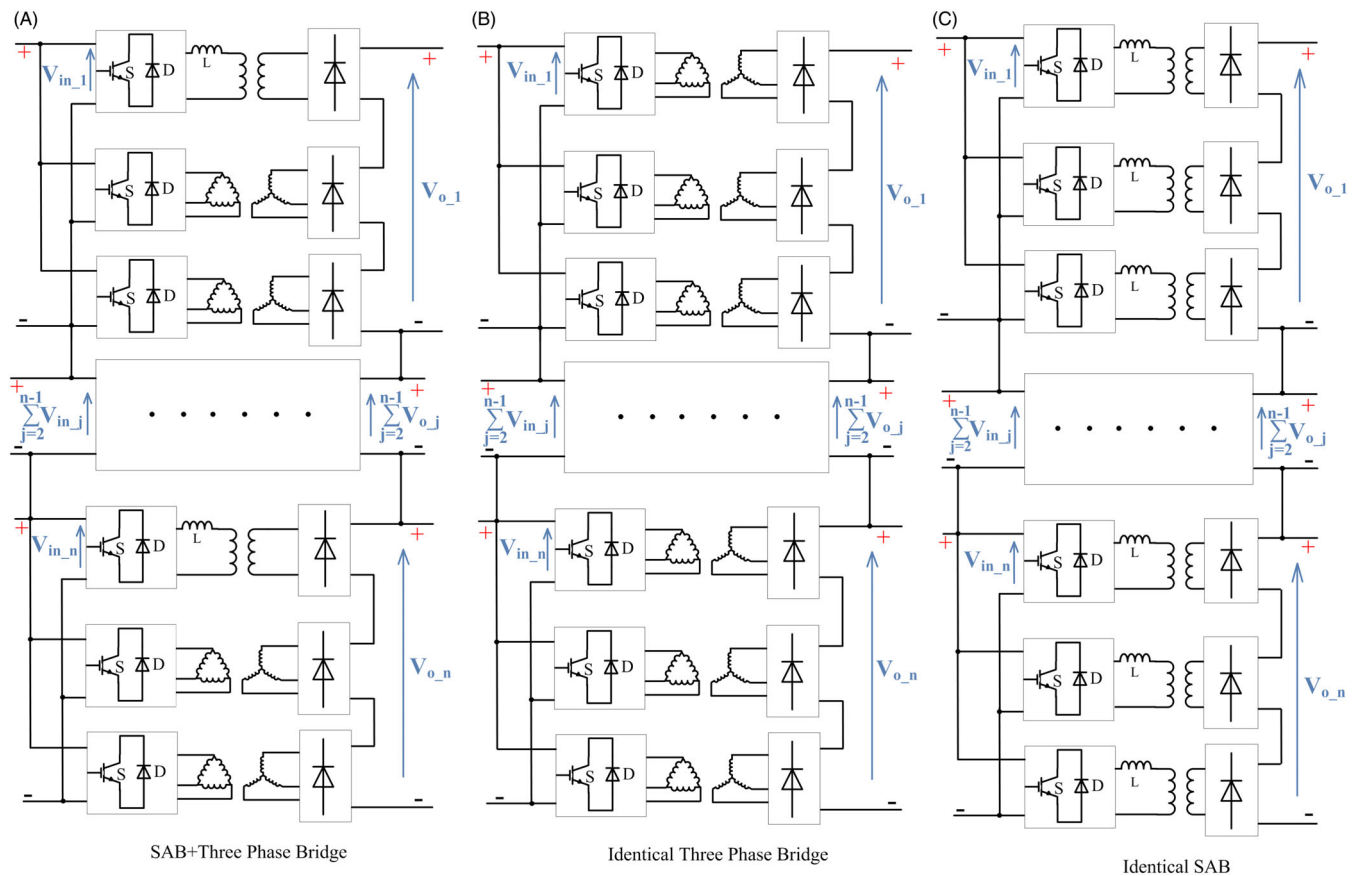


FIGURE 4 Three different unidirectional ISIPOS converter structures

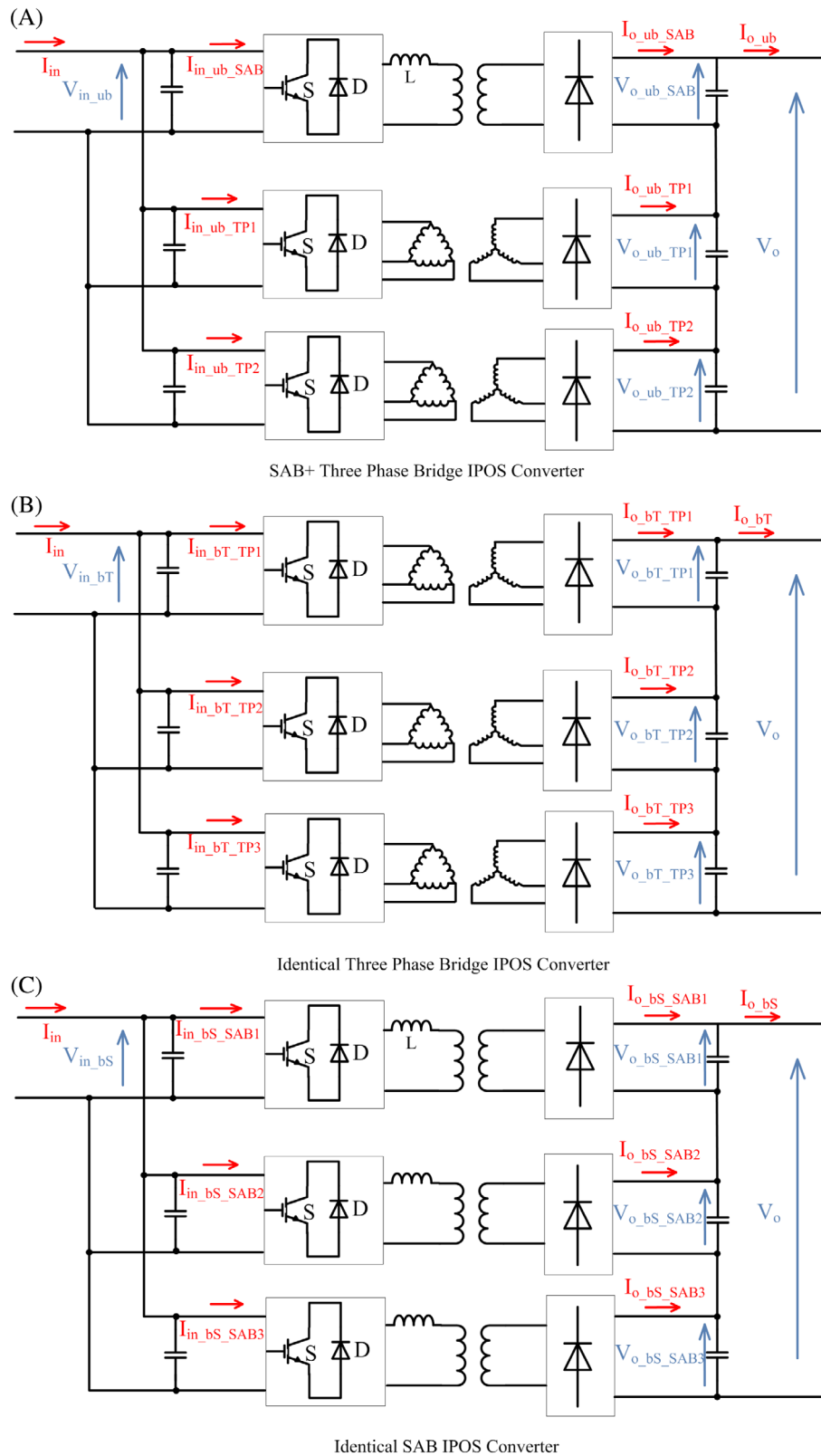


FIGURE 5 Three different unidirectional IPOS converter Structures

1. In the multi-terminal HVDC system in Figure 1, the wind turbine (include PMSG) at the very beginning of the sending end can be regarded as the equivalent current source, while the onshore power system at the receiving end should be treated as a voltage source. Against this backdrop, all the DC-DC converters in the system should be designed as input voltage controllable converters rather than output voltage controllable ones.¹⁴

TABLE 1 Operating parameters of three different unidirectional IPOS converters

50 kV-400 kV 30 MW IPOS converter				
	SAB + three-phase bridge			
	SAB converter	Three-phase bridge converter	Identical three-phase bridge	Identical SAB
Switching frequency	2 kHz	2/3 kHz	2/3 kHz	2 kHz
turns ratio	$N_1:N_2 = 1:1.18$	$N_1:N_2 = 4:7$	$N_1:N_2 = 3:4$	$N_1:N_2 = 1:3.1$
Input voltage	50 kV	50 kV	50 kV	50 kV
Output voltage	50 kV	175 kV	$\frac{400}{3}$ kV	$\frac{400}{3}$ kV
Input capacitor	2.6 μ F	2.6 μ F	2.6 μ F	2.6 μ F
L_p	986 μ H	N/A	N/A	3 mH
Output capacitor	2.6 μ F	2.6 μ F	2.6 μ F	2.6 μ F
k_p	1.435e-3	N/A	N/A	1.152e-3
k_i	0.328	N/A	N/A	0.1064

- The input voltage of the SAB converter with primary side inductor can be controlled easily by PWM control, while that of the Three-Phase Bridge converter shown in Figure 3 cannot be adjusted effectively by duty ratio control.¹⁴ Adding auxiliary components on the circuit (inductor, capacitor, etc.) may improve its controllability, but this increases the cost and size of the components in a large amount. Frequency control will also add difficulty to the design and manufacture of the galvanic isolated converter. However, the advantages of the Three-Phase Bridge converter in a high-power high-voltage system should not be ignored, so the open-loop controlled Three-Phase Bridge converter is put into the system for further research, and its feasibility is proved in Reference 14.
- Each IPOS block in Figure 4A (eg, the IPOS block with input voltage V_{in_1}) is constituted of a SAB converter (Figure 2) and two Three-Phase Bridge converters (Figure 3). This structure is able to have partial input voltage control, as well as inheriting the advantages of the Three-Phase Bridge converter.
- Each IPOS block in Figure 4B consists of three Three-Phase Bridge converters (Figure 3), and the whole ISIPOS structure is balanced but open-loop controlled.
- Each IPOS block in Figure 4C consists of three SAB converters (Figure 2), and the whole ISIPOS structure is balanced and the input voltage can be fully controlled.
- The number of individual converters in each of the IPOS block can be varied according to requirements when building the system in the real world. In this study, the number is set to be 3.

3 | MODELLING OF THE THREE DIFFERENT UNIDIRECTIONAL IPOS CONVERTER

In Figure 1, the ISIPOS converter is used to collect the power from the whole wind farm and step up the voltage. The 200 to 1000 MW ISIPOS converter in Figure 1 is reduced to a 15/30 MW converter in this modelling, which means the value of n in Figure 4 can be much smaller than that in reality. If n is set to be larger than 1, the system simulation requirements may exceed the ability of the software. Because increasing the value of n only reduces the I/O voltage and power of each identical IPOS block, setting $n = 1$ is a reasonable choice as it will not change the simulation results significantly or influence the overall performance of the high-power, high-voltage ISIPOS converter in the system.

Figure 5 shows more detailed circuit diagrams of these three different ISIPOS converter structures when $n = 1$, or say, three different IPOS structures, and all the simulation and hardware studies of the converter in this paper are based on this figure.

The circuit parameters of these three different unidirectional IPOS converters are given in Table 1. The design procedures of an SAB converter are given in References 14,18, so all the circuit and control parameters for the converters are presented directly in Table 1. The turns ratio of the Three-Phase Bridge converters is calculated according to the requirements of the IPOS converter and the turns ratio of the SAB converter, while the detailed study of the high-power Three-Phase Bridge converter can be seen in Reference 14.

In this study, each converter in Figure 5 needs to handle a relatively high voltage and high power, so all the electrical components should be regarded as equivalent components rather than the real ones.

3.1 | Turns ratio

In the system, the input voltage of the IPOS converter is about 50 kV, while the output voltage is set to be 400 kV. For the balanced Identical Three-Phase Bridge IPOS converter with delta-star transformer, the turns ratio $N_2:N_1$ (n_{TP_b}) can be calculated as follows:

$$n_{TP_b} = \frac{400}{3 \times 2 \times 50} = 4 : 3$$

For the SAB + Three-Phase Bridge IPOS converter, the turns ratio of each sub-converter should be designed according to the required controllability. If the turns ratio of the SAB converter is relatively small, its output voltage can only take a small portion of the total output voltage V_o (Figure 5). In this situation, the output voltage ripple of each converter can be reduced at the cost of poorer controllability of the IPOS structure. If the turns ratio of the SAB converter is increased, the whole ISIPPOS structure can withstand a more extensive voltage fluctuation range, but the voltage ripple may also increase. In summary, the design of the turns ratio should depend on the stability of the receiving end system. In this simulation, the output voltage of the SAB converter is set to be 50 kV, so Reference 14:

$$n_{SAB_ub}(N_2 : N_1) = 1.18 : 1$$

$$n_{TP_ub}(N_2 : N_1) = \frac{350}{2 \times 2 \times 50} = 7 : 4$$

n_{SAB_ub} indicates the turns ratio of the SAB converter in the SAB + Three-Phase Bridge IPOS converter structure, while n_{TP_ub} is the turns ratio of the Three-Phase Bridge converter in the SAB + Three-Phase Bridge IPOS converter structure.

3.2 | Switching frequency

Taking the core material of high-power transformers into consideration, the switching frequency of the SAB converter in this IPOS structure is set to be 2 kHz, which is the same as that for the multi-connected 5 MW SAB converter in Figure 1.²⁰⁻²³ In the real world, a 5 kV input 5 MW SAB converter is a reasonable choice for the ISIPPOS converter. Hence, 2 kHz is an appropriate switching frequency. The voltage/power rating of the converter is increased in simulation to be many times larger than in reality to reduce the number of converters in the simulation to a reasonable

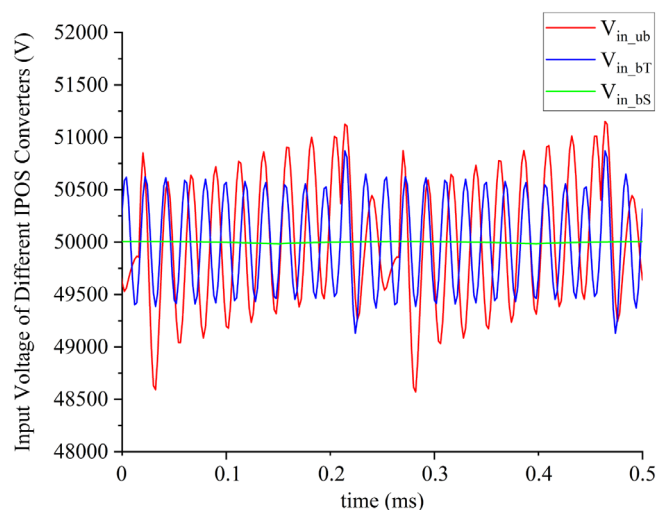


FIGURE 6 Input voltage of three different IPOS converter. V_{in_ub} , input voltage of SAB + three-phase bridge IPOS converter; V_{in_bT} , input voltage of identical three-phase bridge IPOS converter; V_{in_bs} , input voltage of identical SAB IPOS converter

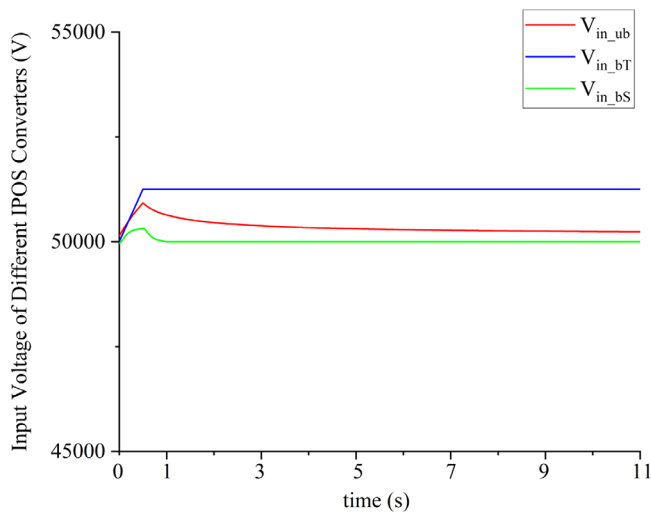


FIGURE 7 Input voltage of three different IPOS converters in long period

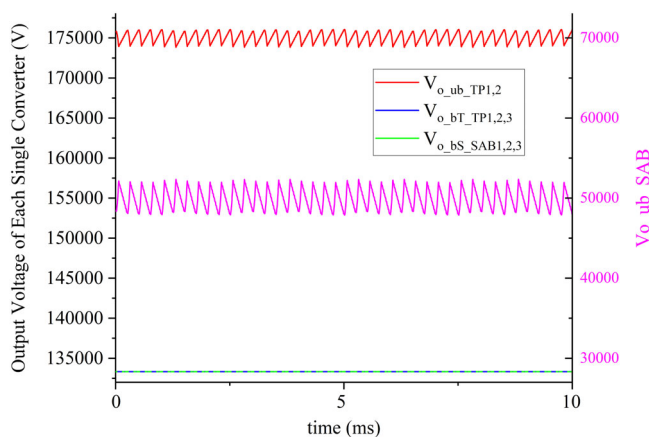


FIGURE 8 Output voltage of each sub converter in balanced and unbalanced IPOS converters. $V_{o_ub_SAB}$, Output voltage of the SAB converter in SAB + three-phase bridge IPOS converter structure; $V_{o_ub_TP1,2}$, output voltages of the three-phase bridge converters in SAB + three-phase bridge IPOS converter structure; $V_{o_bT_TP1,2,3}$, output voltages of the three-phase bridge converters in identical three-phase bridge IPOS converter structure; $V_{o_bs_SAB1,2,3}$, output voltages of the SAB converters in identical SAB IPOS converter structure

number, and all the “equivalent component parameters” are increased or decreased also to match the rating of the converter. However, the switching frequency of the converter should be set to a realistic value to keep the correct operating properties of the converter.

The switching frequency of the Three-Phase Bridge converter in the simulation model is set to be 667 Hz, to leave a margin from the upper frequency limit of silicon steel/iron,^{20,23–28} as well as synchronize its output ripple frequency with that of the SAB converter, which may be connected in series with it.

3.3 | Input and output capacitor

In the simulation of the individual IPOS converter, both the input and output capacitors are selected to be $2.6 \mu\text{F}$.¹⁷ It is a small enough value that can realistically be used in the application for the high-power high-voltage system, and the simulation results illustrate that both the input and output voltage ripple are limited within an acceptable range on the single IPOS simulation. The value of both input and output capacitors of the IPOS converter can be varied during the whole system simulation study (simulation study of the system shown in Figure 1).

4 | SIMULATION OF THE THREE DIFFERENT UNIDIRECTIONAL IPOS CONVERTERS

In this section, all the simulation parameters are based on Figure 5. I_{in} is a 600 A current source, which is the nominal input current for the IPOS converter when six turbines are connected in the system; V_o is a 400 kV voltage source, which is the output voltage rating of the IPOS converter.

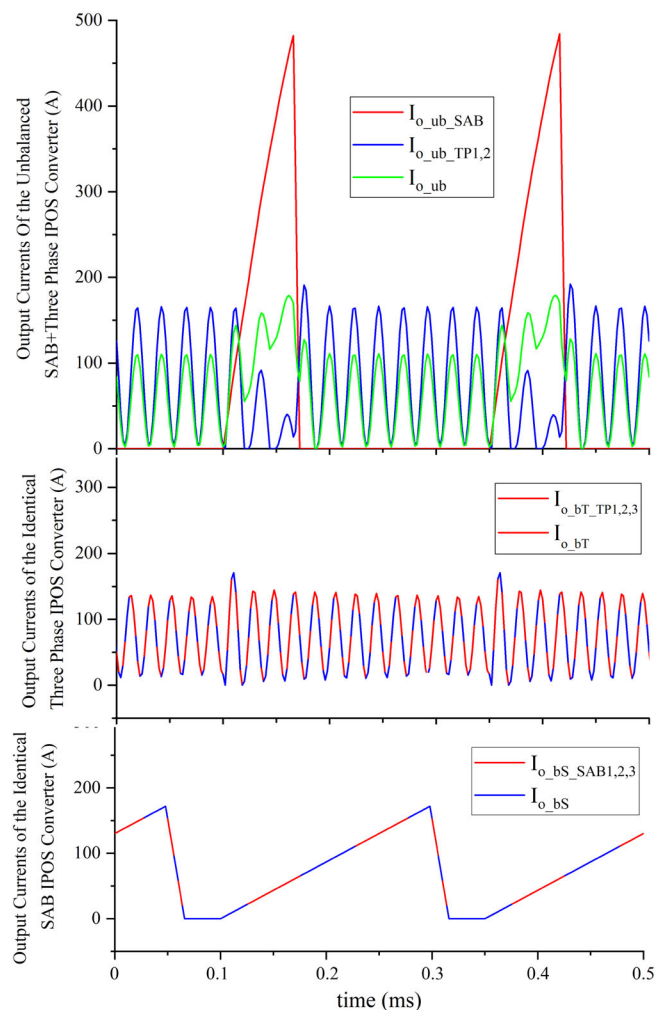


FIGURE 9 Output currents of balanced and unbalanced IPOS converters

4.1 | Input voltage V_{in_ub} , V_{in_bT} and V_{in_bs}

Figure 6 shows the input voltage waveform of three different unidirectional IPOS converters in steady state. It can be seen that the voltage ripple of the Identical Three-Phase Bridge IPOS converter is a little bit smaller than that of the unbalanced one, while that of the full controlled Identical SAB converter is much smaller than the others. The balanced converters have a lower ripple.

The peak-to-peak value of the voltage ripple content and fast Fourier transform algorithm (FFT) analysis are not discussed in this paper, as a more valuable and comprehensive discussion can be given when putting these IPOS converters into a separate system study.

Figure 7 displays the DC component of V_{in_ub} , V_{in_bT} and V_{in_bs} over a relatively longer period to illustrate the different performances of partly controllable, uncontrollable and fully controllable converters when the onshore system voltage (output side of the converter) fluctuates. In this simulation, the output voltage jumps from 400 to 410 kV after 1 second.

As expected, the input voltage value of the uncontrollable Three-Phase Bridge IPOS converter increases with the increase of the output voltage, while that of the controllable converters returns to 5 kV after a few tens of seconds. It also can be observed that the fully controllable IPOS converter is more robust than the partly controllable converter, as it not only has a lower transient state peak but also goes back to the desired value faster.

4.2 | Output voltage

Figure 8 shows the waveforms of $V_{o_ub_SAB}$, $V_{o_ub_TP1}$, $V_{o_ub_TP2}$, $V_{o_ub_TP3}$, $V_{o_bT_TP1}$, $V_{o_bT_TP2}$, $V_{o_bT_TP3}$, $V_{o_bs_SAB1}$, $V_{o_bs_SAB2}$ and $V_{o_bs_SAB3}$ under the steady state. As expected, the output voltages from Identical SAB or Three-Phase Bridge IPOS

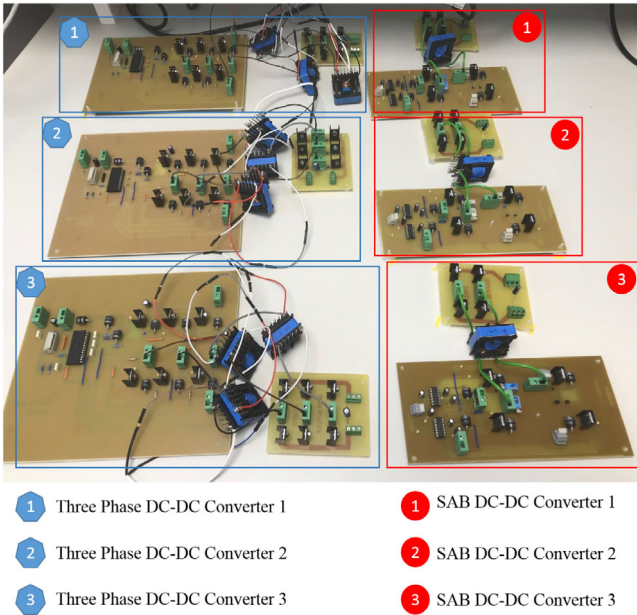


FIGURE 10 The prototype of the three-phase bridge DC-DC converters and the SAB DC-DC converters

Input voltage	≈4.5 V
Input current	≈2.5 A
Output voltage	≈ 12 V
Switching frequency of SAB converter	62.5 kHz
Switching frequency of three-phase bridge converter	20.3 kHz

TABLE 2 Operating parameters of the downscaled IPOS DC-DC converters

converters are the same. The output voltage ripple content of the Three-Phase Bridge converters in unbalanced structure can be regarded as the compensation for the ripple content of SAB converter, while the outputs from the balanced structure are much more ideal and can be treated as zero THD.

4.3 | Output current

The output current waveform of these converters can be seen in Figure 9. For the unbalanced converter, the output voltage and the output current of the Three-Phase Bridge converter are also influenced by that of the SAB converter, as well as I_{o_ub} . For the balanced converter, the output currents of the Three-Phase Bridge converters $I_{o_bT_TP1,2,3}$ are the same as the final output current I_{o_bT} , while the output currents of the SAB converters $I_{o_bS_SAB1,2,3}$ are the same as the final output current I_{o_bS} . This result means in balanced converter structures, the dependency on the filter may be less, or smaller output capacitors may be needed to limit the ripple content.

In Figure 9:

$I_{o_ub_SAB}$: Output current of the SAB converter in SAB + Three-Phase Bridge IPOS converter structure.

$I_{o_ub_TP1,2}$: Output currents of the Three-Phase Bridge converters in SAB + Three-Phase Bridge IPOS converter structure.

I_{o_ub} : Output current of the SAB + Three-Phase Bridge IPOS converter.

$I_{o_bT_TP1,2,3}$: Output currents of the Three-Phase Bridge converters in Identical Three-Phase Bridge IPOS converter structure.

I_{o_bT} : Output current of the Identical Three-Phase Bridge IPOS converter.

$I_{o_bS_SAB1,2,3}$: Output currents of the SAB converters in Identical SAB IPOS converter structure.

I_{o_bS} : Output current of the Identical SAB IPOS converter.

According to all the simulation results of the three different unidirectional IPOS converters, the overall performances of the balanced identical converters are better than that of the unbalanced converter. The waveform ripple content of the balanced converter is always smaller than that of the unbalanced converter. The simulation results in this section are aimed at providing an understanding of the operation property of the IPOS converters themselves, while their performance on the system can have some differences, and the more detailed comparison will be discussed in the authors' other papers.

TABLE 3 Operating parameters of the SAB converter in transient state

Initial output voltage	13.2 V
Input current	0.9 A
Desired input voltage	12.6 V
Frequency	62.5 kHz
Transformer turns ratio N2:N1	1.4
First transient state	Step input current
Second transient state	Sudden output voltage drop

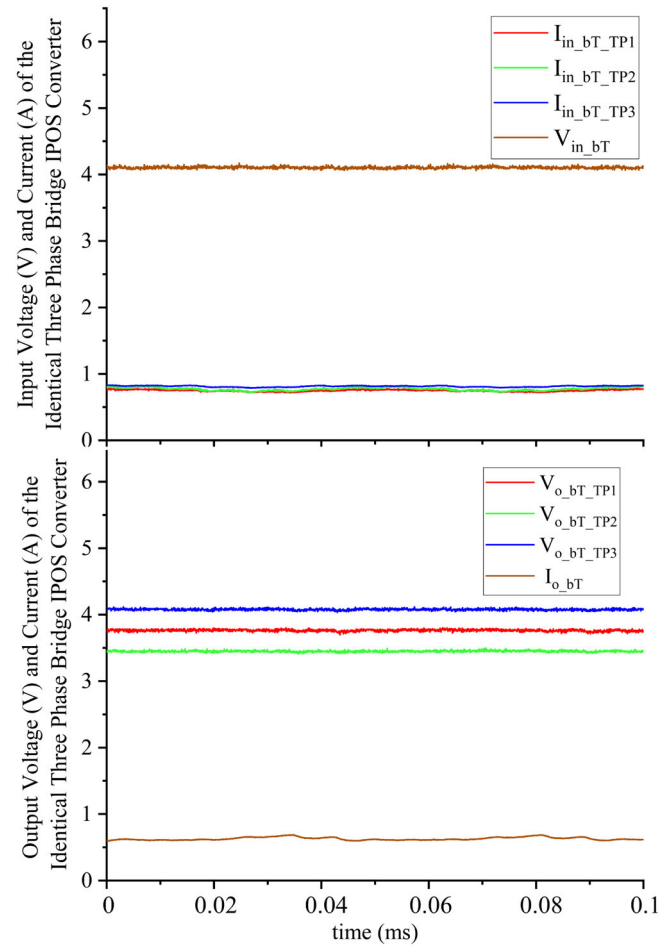


FIGURE 11 Input and output waveforms of the identical three-phase bridge IPOS Converter

5 | DOWNSCALED HARDWARE STUDY OF THE THREE DIFFERENT UNIDIRECTIONAL IPOS CONVERTER

In this section, the downscaled hardware test of the three different IPOS converters is given to verify the operability of these converters. The current and voltage waveforms from the hardware tests do not match the simulation results of the high-power system completely, due to the enormous power and voltage differences. The prototype of all the converters can be seen in Figure 10. The Three-Phase Bridge DC-DC converter 1, 2 and 3 can constitute the Identical Three-Phase Bridge IPOS converter, the SAB DC-DC converter 1, 2 and 3 can constitute the Identical SAB IPOS converter, while the SAB DC-DC converter 1 and Three-Phase Bridge DC-DC converter 2 and 3 can constitute the SAB + Three-Phase Bridge IPOS converter. During the operation, a DC battery with voltage level of around 12 V is connected to the output of each of the structure to mimic the onshore power grid connected at the receiving end of the system in Figure 1. The operating parameters of these three different IPOS converter structures can be seen in Table 2.

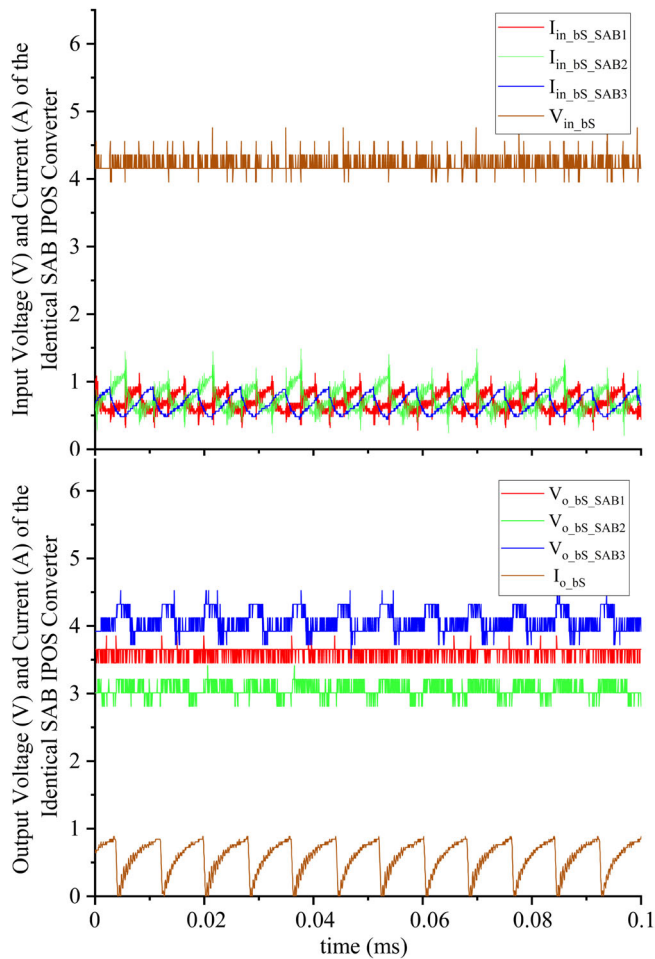


FIGURE 12 Input and output waveforms of the identical SAB IPOS converter

5.1 | Steady state comparison

In this section, based on Figure 5, both the input and output waveforms of the three different converters are presented, shown in Figures 11-13. From these three figures, it can be seen that all three structures can operate as expected, especially the unbalanced SAB + Three-Phase Bridge IPOS converter. Based on the turns ratio of the transformers in Tables A1 and A2, the ratio of $V_o:V_{in}$ should be more or less the same in each of the single converters, which means both the input current and output voltage can be shared equally. From these three figures, in each of the IPOS converters, the three input currents can be regarded as equal to each other. However, as the parameters of some of the components, like transformers or the length of the connection wire, are not exactly the same, the output voltage of each converter can vary.

The control signals for the three IPOS SAB converters in Figure 5C have 120° phase shift between each other in the downscaled hardware test. This phase shift in the SAB IPOS converter reduces the ripple content very substantially.

When looking into the ripple content of both input and output voltage/current waveform, the ability of the SAB converter to limit the ripple content is much less than that of the Three-Phase Bridge DC-DC converter. This phenomenon is not obvious in the simulation results of the high-power converters themselves, but when putting all these three IPOS structures into the high-voltage system in Figure 1, this advantage of the Three-Phase Bridge DC-DC converter can be displayed.¹⁴

Finally, in this hardware test, the efficiency of all these IPOS converters is low, only around 60%. The low voltage rating of these converters make the voltage drop or losses on components like diodes become significant, which will not be the case in the high-power system.

5.2 | Transient state test of the SAB converter

The transient state test of the SAB DC-DC converter is given in this part to identify its input voltage controllable feature. The operating parameters of the converter under this transient state test can be concluded in Table 3. A step

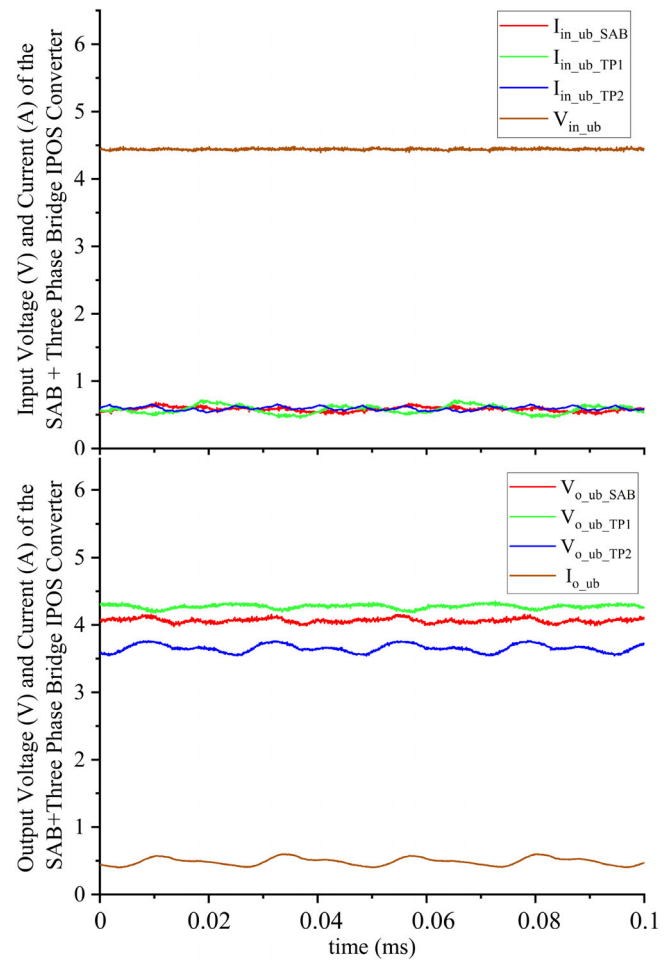


FIGURE 13 Input and output waveforms of the SAB + three-phase bridge IPOS converter

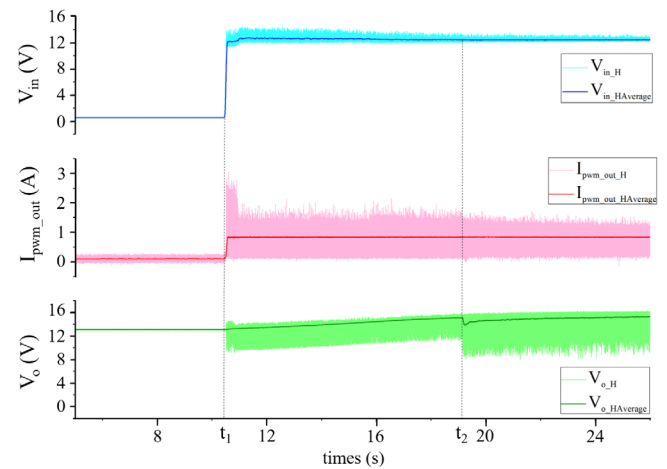


FIGURE 14 Transient state performance of the SAB DC-DC converter

current of 0.9 A is generated from the equivalent DC current source, while 13.2 V is the initial voltage of the DC battery connected at the output of the converter.

It should be noted that the input current source is approximated by the current limit mode of a DC power supply.

In order to monitor the transient performance of the converter, Dewesoft-SIRIUS, which can record signals over a long period of time, is used to record the waveform. The sample rate of the Dewesoft-SIRIUS is much slower than that of the digital oscilloscope, which leads to a significant distortion of the waveform if monitored in detail. However, when looking at the waveform over a long period of time, Dewesoft-SIRIUS is able to record the trend, despite the fact that some of the higher frequency detail is lost.

Taking the circuit diagram of the SAB converter in Figure 2 as reference, the waveforms of V_{in} , I_{pwm_out} and V_o over a relatively long period of time compared with the switching period of 16 μ s can be seen in Figure 14. The average value

of the waveform based on a 0.05 second time period is given as well as the original waveform to reduce the influences caused by the noise to provide a clear view of the dynamic performance of the waveform.

At t_1 , a step input current occurs, increasing from 0 to 0.9 A. The control loop monitors the input voltage and tries to reduce the error by varying the duty ratio. Between t_1 and t_2 , the output voltage V_o is increasing gradually, as the DC battery is continually charged when the converter is operating. This is also increasing the time needed for V_{in} to reach its desired value. At t_2 , a sudden voltage drop at the output is forced into the circuit, and the input voltage is still controlled well at the desired voltage, although the reaction of the control circuit is not reflected clearly in the waveform diagram, due to the slow sample rate of the equipment and the relatively small output voltage drop.

6 | CONCLUSION

This paper studies the operation of three different IPOS converter structures, which can be applied in high-power offshore wind farm based DC systems. As well as two structures composed with identical DC-DC converters, a novel IPOS converter constituted by different converter types, which may inherit the advantages of the different converters, is also studied in this paper. In the simulation results, the advantages of the Three-Phase Bridge converter on the limitation of the ripple content is not obvious, and this is due to the ideal input current source. Combining the simulation results and the downscaled hardware test, the operating property of these three different IPOS converter structures are as expected. That said, the study of the converter itself has limitations. For example, in reality, the input of the converter is not an ideal current source and more accurate performance of the converters has yet to be studied in the system. All three IPOS converter structures have their advantages and disadvantages, which are listed below, and the final application should depend on their performance in the system.

- Compared with the SAB DC-DC converter, the Three-Phase Bridge DC-DC converter performs better on the limitation of the current and voltage ripple content. In an IPOS-connected converter structure, the more Three-Phase Bridge converter applied, the lower ripple content can be obtained.
- The IPOS converter structure with more Three-Phase Bridge DC-DC converter can have higher power transfer ability.
- The IPOS structure with more fully controlled SAB DC-DC converter can be more robust to the voltage fluctuation.

ACKNOWLEDGEMENTS

The authors would like to express their sincere gratitude to the University of Edinburgh school of Engineering technical staff Mr Kevin Tierney, Mr Douglas Carmichael, Mr Iain Gold, Mr Jamie Graham, Mr Alasdair Christie for their help on making PCBs and giving technical guidance in this research.

CONFLICT OF INTEREST

The authors declare no conflict of interest.

PEER REVIEW

The peer review history for this article is available at <https://publons.com/publon/10.1002/2050-7038.12855>.

DATA AVAILABILITY STATEMENT

The data that support the findings of this study are available from the corresponding author upon reasonable request.

ORCID

Jonathan K. H. Shek  <https://orcid.org/0000-0001-5734-2907>

REFERENCES

1. IRENA. *Innovation Outlook: Offshore Wind*. Abu Dhabi: International Renewable Energy Agency; 2016.
2. Tang G. Introduction. *Voltage Source Converter Based High Voltage Direct Current Technology*. 1st ed. Beijing, China: China Electric Power Press; 2010:1-26.
3. Why HVDC — Technical Advantages. <http://new.abb.com/systems/hvdc/why-hvdc/technical-advantages>. Accessed July 27, 2017.
4. Roland R, Łukasz S. Evolution of the HVDC link connecting offshore wind farms to onshore power systems. *Energies*. 2020;13(1):1914.
5. Rong X, Macpherson DE, Shek JKH. The effect of high power DC-DC converter in offshore multi-terminal medium and high voltage DC networks. Paper presented at: International Conference on Renewable Power Generation (RPG 2015); October 17-18, 2015; Beijing, China:1-6.

6. Sun K, Li K, Lee W, et al. VSC-MTDC system integrating offshore wind farms based optimal distribution method for financial improvement on wind producers. *IEEE Trans Ind Appl.* 2019;55(3):2232-2240.
7. Páez JD, Frey D, Maneiro J, Bacha S, Dworakowski P. Overview of DC–DC converters dedicated to HVdc grids. *IEEE Trans Power Delivery.* 2019;34(1):119-128.
8. Shi G, Cai X, Sun C, Chang Y, Yang R. All-DC offshore wind farm with parallel connection: an overview. Paper presented at: 12th IET International Conference on AC and DC Power Transmission (ACDC 2016); May 28-29, 2016; Beijing, China:1-6.
9. Yin R, Shi M, Hu W, Guo J, Hu P, Wang Y. An accelerated model of modular isolated DC/DC converter used in offshore DC wind farm. *IEEE Trans Power Electron.* 2019;34(4):3150-3163.
10. Guan M. A series-connected offshore wind farm based on modular dual-active-bridge (DAB) isolated DC–DC converter. *IEEE Trans Energy Convers.* 2019;34(3):1422-1431.
11. Haileselassie T, Uhlen K, Tande JO, Anaya-Lara O. Connection scheme for north sea offshore wind integration to UK and Norway: power balancing and transient stability analysis. Paper presented at: 2011 IEEE Trondheim PowerTech; June 19-23, 2011; Trondheim, Norway:1-5.
12. Wang H, Ma KW. IGBT technology for future high-power VSC-HVDC applications. Paper presented at: 12th IET International Conference on AC and DC Power Transmission (ACDC 2016); May 28-29, 2016; Beijing, China:1-6.
13. Bahmani MA, Thiringer T, Rabiei A, Abdulahovic T. Comparative study of a multi-MW high power density DC transformer with an optimized high frequency magnetics in all-DC offshore wind farm. *IEEE Trans. Power Delivery.* 2016;31(2):857-866.
14. Rong X. The Study of the Offshore Wind Farm Based Multi-Terminal DC System and the Application of High Power DC-DC Converters [PhD thesis]. University of Edinburgh; 2018.
15. You J, Cheng L, Fu B, Deng M. Analysis and control of input-parallel output-series based combined DC/DC converter with modified connection in output filter circuit. *IEEE Access.* 2019;7(1):58264-58276.
16. Max L, Lundberg S. System efficiency of a DC-DC converter based wind farm. *Wind Energy.* 2008;11(1):109-120.
17. Park K, Chen Z. Control and dynamic analysis of a parallel connected single active bridge DC–DC converter for DC-grid wind farm application. *IET Trans Power Electron.* 2015;8(5):665-671.
18. Kim H, Yoon C, Choi S. A three-phase DC-DC converter for fuel cell applications. Paper presented at: 2008 IEEE Power Electronics Specialists Conference; August 2008; Rhodes, Greece:1290-1295.
19. Tang Y, Luo Y, Liang Y. Magnetic circuit. *Electromechanics.* 3rd ed. Beijing, China: China Machine Press; 2008:31-54.
20. Keke L, Lin L. Analysis of favored design frequency of high-frequency transformer with different power capacities. Paper presented at: 2014 International Conference on Power System Technology; October 20-22, 2014; Chengdu, China:2272-2278.
21. Dincan C, Kjaer P, Chen Y, Munk-Nielsen S, Bak CL. Analysis of a high-power, resonant DC–DC converter for DC wind turbines. *IEEE Trans Power Electron.* 2018;33(9):7438-7454.
22. Soltan NJ. High-Power Medium-Voltage DC-DC Converters: Design, Control and Demonstration [PhD thesis]. Rwth Aachen University; 2017.
23. Shen W, Wang F, Boroyevich D, Tipton CW. Loss characterization and calculation of nanocrystalline cores for high-frequency magnetics applications. *IEEE Trans Power Electron.* 2008;23(1):475-484.
24. Komatsubara M, Sadahiro K, Kondo O, Takamiya T, Honda A. Newly developed electrical steel for high-frequency use. *J. Magn. Magn. Mater.* 2002;242(1):212-215.
25. Constantinides S. Designing with thin gauge. Paper presented at: SMMA Fall Technical Conference; October 2008; Munich, Germany.
26. Reass WA, Baca DM, Doss JD, Gribble RF. Design technology of high-voltage multi-megawatt polyphase resonant converter modulators. Paper presented at: IECON'03. 29th Annual Conference of the IEEE Industrial Electronics Society; November 2-6, 2003; Roanoke, VA:96-101.
27. Heinemann L. An actively cooled high power, high frequency transformer with high insulation capability. Paper presented at: 17th Annual IEEE Applied Power Electronics Conference and Exposition; March 10-14, 2002; Dallas, TX:352-357.
28. Inoue S, Akagi H. A bidirectional isolated DC-DC converter as a core circuit of the next-generation medium-voltage power conversion system. *IEEE Trans Power Electron.* 2007;22(2):535-542.

How to cite this article: Rong X, Shek JKH, Macpherson DE. The study of different unidirectional input parallel output series connected DC-DC converters for wind farm based multi-connected DC system. *Int Trans Electr Energy Syst.* 2021;31:e12855. <https://doi.org/10.1002/2050-7038.12855>

APPENDIX A.

Transformer parameters of the hardware models of converters

In the hardware testing in this paper, three downscaled Three-Phase Bridge converters and another three downscaled SAB converters altogether were designed and built by the author. For each of the Three-Phase Bridge converters, three single transformers are connected together as a Three-Phase transformer, while single-phase transformers are applied in each of the SAB converters. The leakage inductance of the transformers used for the SAB converters is designed to take the place of the extra inductance L_p at the primary side of the converter in Figure 2. In this section, the parameters of these transformers are listed in Tables A1 and A2, based on the equivalent circuit of a single-phase transformer in Figure A1. All the transformers were hand made by the author, so their parameters are not entirely identical, but similar.

TABLE A1 Transformer parameters of the three-phase bridge DC-DC converters in hardware model

Transformer parameters of the three-phase bridge converter 1			
	Phase A	Phase B	Phase C
Switching frequency	20.3 kHz	20.3 kHz	20.3 kHz
$L_1(\mu\text{H})$ and $R_1(\text{m}\Omega)$	$L = 1.65$ $R = 81.3$	$L = 1.31$ $R = 73$	$L = 1.77$ $R = 87.4$
$L_2(\mu\text{H})$ and $R_2(\text{m}\Omega)$	$L = 0.8$ $R = 32$	$L = 0.57$ $R = 28$	$L = 0.72$ $R = 35.7$
Turns ratio $N_s:N_p$	0.663	0.663	0.663
$(L_2:L_1):(N_s:N_p)^2$	1.1	0.99	0.92
Parallel $L_m(\mu\text{H})$ and $R_m(\Omega)$	$L = 140$ $R = 198$	$L = 138$ $R = 197$	$L = 136$ $R = 547$
Transformer parameters of the three-phase bridge converter 2			
	Phase A	Phase B	Phase C
Switching frequency	20.3 kHz	20.3 kHz	20.3 kHz
$L_1(\mu\text{H})$ and $R_1(\text{m}\Omega)$	$L = 0.65$ $R = 30.7$	$L = 0.7$ $R = 29$	$L = 0.755$ $R = 30.3$
$L_2(\mu\text{H})$ and $R_2(\text{m}\Omega)$	$L = 0.28$ $R = 10.2$	$L = 0.33$ $R = 9.5$	$L = 0.343$ $R = 11.9$
Turns ratio $N_s:N_p$	0.664	0.664	0.663
$(L_2:L_1):(N_s:N_p)^2$	0.98	1.07	1.03
Parallel $L_m(\mu\text{H})$ and $R_m(\Omega)$	$L = 128$ $R = 205$	$L = 120$ $R = 214$	$L = 112$ $R = 208$
Transformer parameters of the three-phase bridge converter 3			
	Phase A	Phase B	Phase C
Switching frequency	20.3 kHz	20.3 kHz	20.3 kHz
$L_1(\mu\text{H})$ and $R_1(\text{m}\Omega)$	$L = 0.77$ $R = 33$	$L = 0.86$ $R = 31$	$L = 0.75$ $R = 33$
$L_2(\mu\text{H})$ and $R_2(\text{m}\Omega)$	$L = 0.32$ $R = 17$	$L = 0.41$ $R = 11$	$L = 0.36$ $R = 13$
Turns ratio $N_s:N_p$	0.664	0.663	0.663
$(L_2:L_1):(N_s:N_p)^2$	0.94	1.08	1.09
Parallel $L_m(\mu\text{H})$ and $R_m(\Omega)$	$L = 126$ $R = 219$	$L = 112$ $R = 228$	$L = 124$ $R = 210$

TABLE A2 Transformer parameters of the SAB DC-DC converters in hardware model

Transformer parameters of the three SAB converters			
	Converter 1	Converter 2	Converter 3
Switching frequency	62.5 kHz	62.5 kHz	62.5 kHz
$L_1(\mu\text{H})$ and $R_1(\text{m}\Omega)$	$L = 1.55$ $R = 103$	$L = 1.55$ $R = 110$	$L = 1.5$ $R = 101$
$L_2(\mu\text{H})$ and $R_2(\text{m}\Omega)$	$L = 3$ $R = 210$	$L = 3$ $R = 218$	$L = 3$ $R = 199$
Turns ratio $N_s:N_p$	1.4	1.4	1.4
$(L_2:L_1):(N_s:N_p)^2$	1	1	1
Parallel $L_m(\mu\text{H})$ and $R_m(\text{k}\Omega)$	$L = 327$ $R = 1.9$	$L = 303$ $R = 1.9$	$L = 298$ $R = 2$

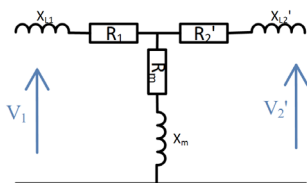


FIGURE A1 Equivalent circuit of a single-phase transformer